Supplementary Materials: Extending Landsat 8: Retrieval of an orange *contra*-band for inland water quality applications

Alexandre Castagna[1]*, Stefan Simis[2], Heidi Dierssen[3], Quinten Vanhellemont[4], Koen Sabbe[1] and Wim Vyverman[1]

S1. Analytical composite *contra*-band retrieval

The analytical *contra*-band possible with OLI band set is a composite band including signals from the turquoise and orange spectral regions. While it is not suitable for applications due to the mixing of the spectral information from those two regions, it serves as a demonstration of the performance of the retrieval when an analytical solution can be used. As noted in the Appendix A of the companion study, analytical retrievals should be performed in radiance space and then converted to reflectance. To apply that approach to the OWT, the OWT cluster average normalized reflectances were first converted to equivalent radiance by using the average simulated clear sky $E_d(\lambda, 0^+)$, and after retrieval of the composite *contra*-band, converted back to reflectance space. Uncertainty as described by the Mean Absolute Percentage Error (MAPE) is 0.4 % for the *in situ* data. In the presence of expected sensor noise, the MAPE increases to 3.88 %, comparable with the mission goal of 3 % maximum error in reflectance. AC error propagate linearly to have about the same magnitude as the red MS band error (slope of 0.994) with a secondary effect of the spectral shape (green to red AC error difference). When AC error is higher in the green than in the red band, AC error in the composite *contra*-band will also be higher than in the red band, by $\approx$ 35 % of the green to red AC error difference. Those retrieval results of the composite band are shown in Fig. S1.

S2. Application of the current OLI orange *contra*-band algorithm to clear waters

As presented in the discussion section of the main study, only turbid waters were included in the calibration of the algorithm to improve performance for those optical conditions where information of cyanobacteria presence is of particular interest. Addition of clear water spectra in the calibration dataset only reduced performance of the algorithm for turbid waters, while not providing improved performance for clear waters without the addition of the blue MS band (described in the next section). Here we further evaluate the performance of the current algorithm when applied to blue-enhanced waters with a variety of conditions from oligotrophic open ocean to optically complex estuaries and fjords in a total of 81 R_{rs} spectra. Those spectra were measured in the Southern Ocean (Kerguelen Islands; October 2016), Santa Barbara Channel (U.S.; October 2015), Monterey Bay and estuarine waters of Elkhorn Slough (U.S.; July 2012) and fjord waters of Svalbard (Norway; May 2013). Southern Ocean data was collected with a bow-mounted spectrometer system (Satlantic, Halifax, Canada) following [1]. Field radiometric data for the other regions was collected with an handheld spectrometer (ASD) with the plaque method for estimation of irradiance [2]. Skyglint was removed with the approach of [3]. The evaluation of algorithm performance shows a general overestimation of the R_{rs}^{orange} (bias of 138 %) across these diverse water types, with non-linearity in the lower signal range (Fig. S2). Despite the poor performance, the coefficient of determination is high since statistics are calculated on a linear scale and most overestimations occur over relatively small reflectance values. The evaluation also shows appropriate performance of the proposed algorithm flag ($R_{rs}^{blue}/R_{rs}^{red} > 2$ and $R_{rs}^{red} < 0.002$ sr^{-1}) to exclude spectra for which large errors are expected (red symbols in Fig. S2B). The spectra for Elkhorn Slough included both turbid waters and optically shallow water over seagrass beds [4], both passing the algorithm flag. For those spectra, the R_{rs}^{orange} was retrieved with a MAPE of 10.5 % (N = 11, data range from 0.0022 to 0.011 sr^{-1}; black symbols in Fig. S2B). Operational methods for filtering shallow water conditions from multispectral data are not yet available.

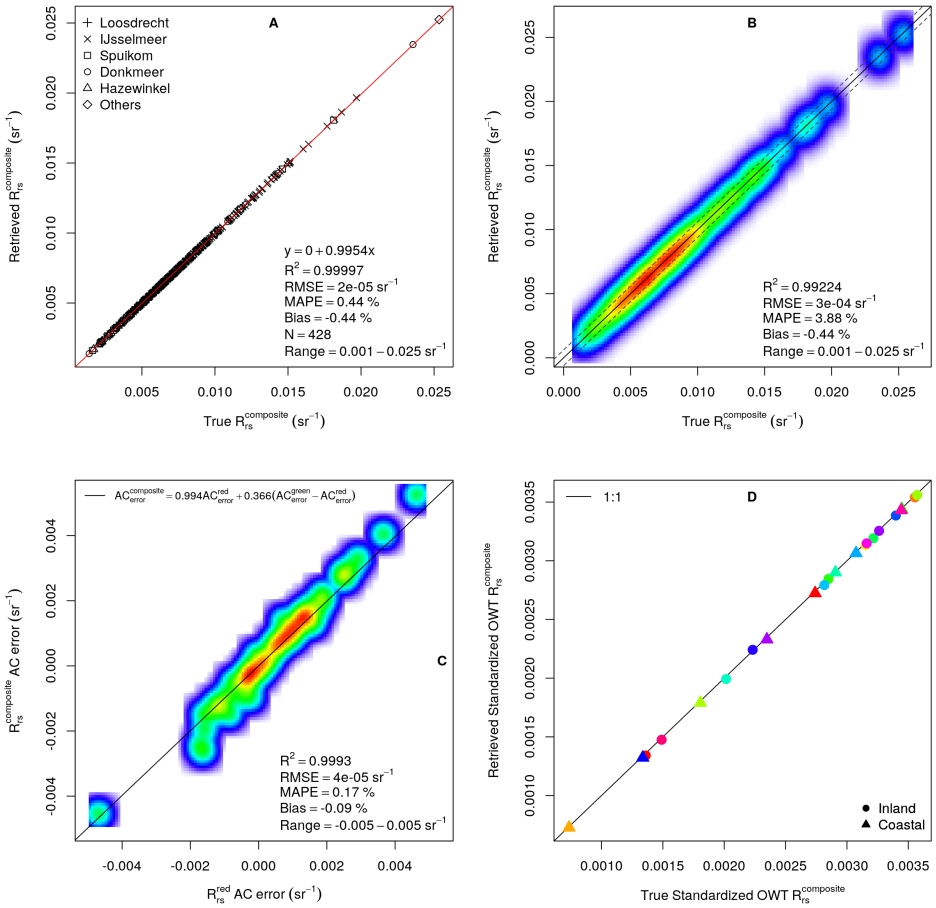

Figure S1. Performance of retrieval of the analytical composite band. (A) The retrieval evaluated with the *in situ* data. (B) Effect of spectrally independent random sensor noise. (C) Spectrally structured AC error propagation compared against red MS band AC error. (D) Retrieval for the OWT cluster averages.

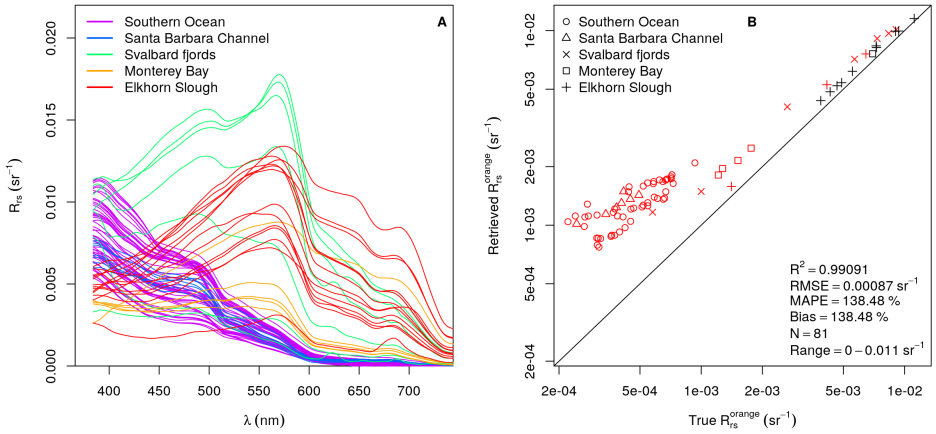

Figure S2. Performance of retrieval of the current OLI orange *contra*-band with clear waters. (A) Clear water spectra sampled in marine and transitional waters. (B) OLI R_{rs}^{orange} retrieval for the clear water spectra. In (B), spectra that would not be processed due to algorithm flag ($R_{rs}^{blue}/R_{rs}^{red} > 2$ and $R_{rs}^{red} < 0.002$ sr^{-1}) is presented in red. Axis in (B) are presented in $\log_{10}$ spacing.

S3. Addition of the blue MS band in the *contra*-band retrieval

The other MS bands can be added to the retrieval algorithm, either explicitly or implicitly. The justification to add more bands is the possibility to accommodate blue-enhanced water spectral shapes together with those of turbid waters, by allowing one or two additional parameters tied to the OLI blue bands. Here the retrievals with the addition of the blue MS band (483 nm) are presented (Fig. S3). Since the blue-enhanced spectra represent a fraction of the total spectra, the fitting allowed for equal weights in both datasets. The MAPE of the retrievals with *in situ* data was 3.87 %, similar to the original dataset. While this suggest no gain in performance compared to the turbid dataset, the extended dataset includes very low values of $R_{\mathrm{rs}}^{\mathrm{orange}}$ that could negatively impact the performance statistics. Indeed the observed an performance is a significant improvement to including blue-enhanced spectra but not the blue MS band (not shown). This gain in performance, however, is overcompensated for in the presence of noise and AC error. In the presence of noise, uncertainty increases to 14.78 % and AC error propagation from the blue band result in increased variability with the AC errors in the adjacent green and red bands, potentially impacting baseline (*e.g.*, OLH) or ratio algorithms for phycocyanin. As can be seen in Fig. S3D, the only OWT cluster not retrieved is the very clear C-2, likely because spectra representative of this cluster were not present in the calibration dataset. To make clear the impact of AC error propagation into the orange *contra*-band when the blue band is included, the lake Erie retrieval is also presented (Fig. S4). Note that the underestimation of the orange signal due to overestimation of turquoise signal from higher undercompensation of atmospheric effects on the blue band when compared with those for the green and red bands result in an increased magnitude of the OLH (and the color scale is changed accordingly). This underestimation of the orange reflectance further intensifies the PC signal in the regions where it is present. However, the Detroit River plume has already enhanced blue reflectance, with the additional AC error propagation, the resulting orange reflectance distance to the green-red baseline is even larger than where PC is present.

S4. OLI to OLCI $R_{\mathbf{rs}}^{\mathbf{orange}}$ comparison per lake

The OLI to OLCI $R_{\mathrm{rs}}^{\mathrm{orange}}$ comparison and performance statistics is shown per lake in Fig. S5. Details on the matchup conditions are presented in Table S1.

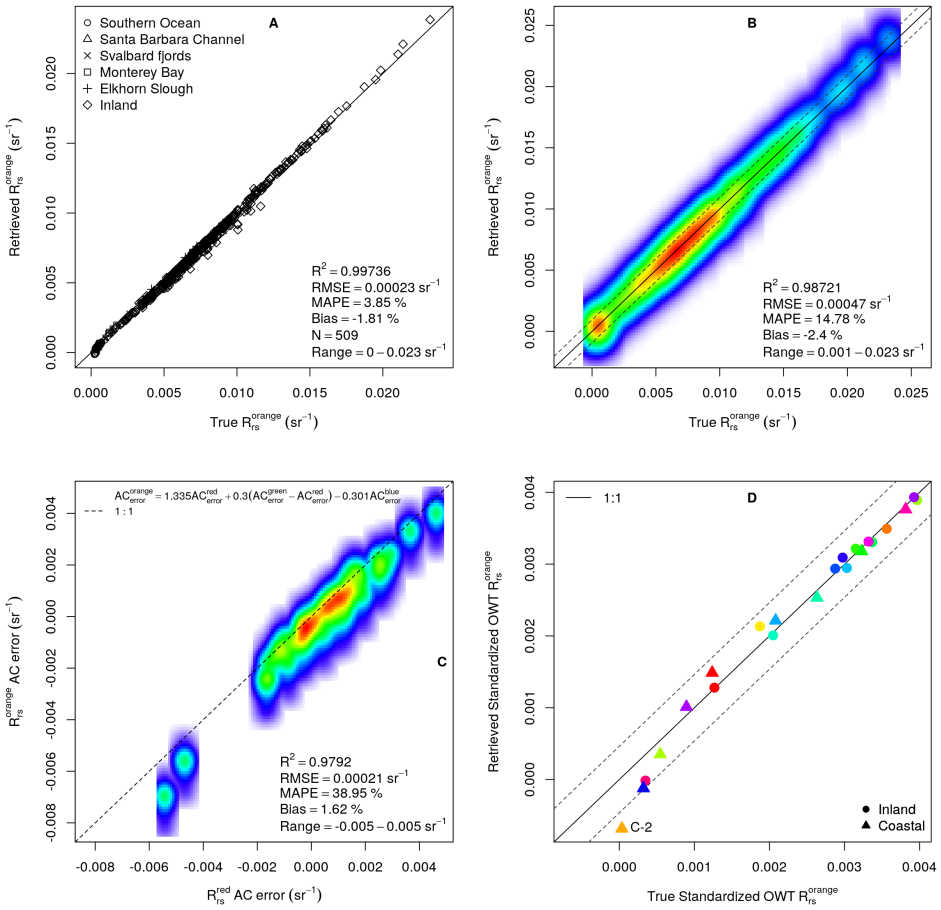

Figure S3. Performance of retrieval of the orange *contra*-band when the blue MS band is also included in the retrieval algorithm. (A) The retrieval evaluated with the *in situ* data. (B) Effect of spectrally independent random sensor noise. (C) Spectrally structured AC error propagation. (D) Retrieval for the OWT cluster averages.

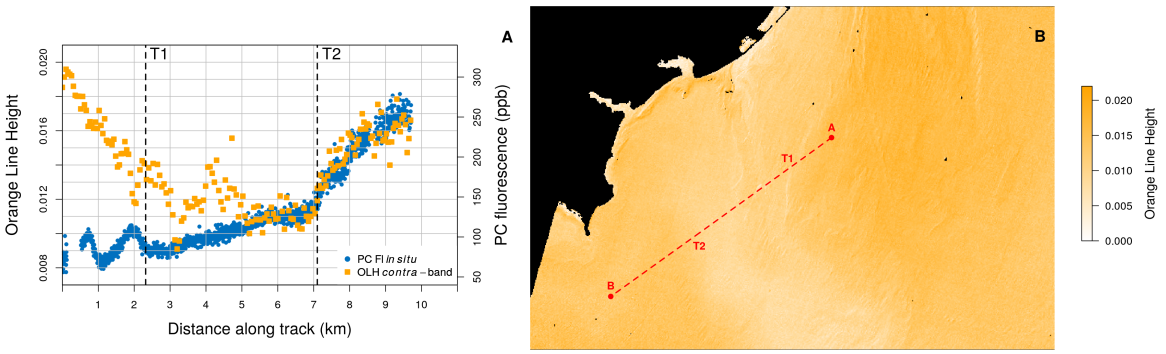

Figure S4. Application of the orange *contra*-band, retrieved with the algorithm including the blue MS band, to calculate the OLH in west Lake Erie. Sampling transect starts in the Detroit River plume at point A and ends at point B in the Maumee Bay, passing through two transition points T1 and T2 [5]. (A) Spatial gradient along the transect line for PC fluorescence and OLH calculated with the *contra*-band algorithm including the blue MS band. (B) OLH calculated with the *contra*-band algorithm that includes the blue MS band.

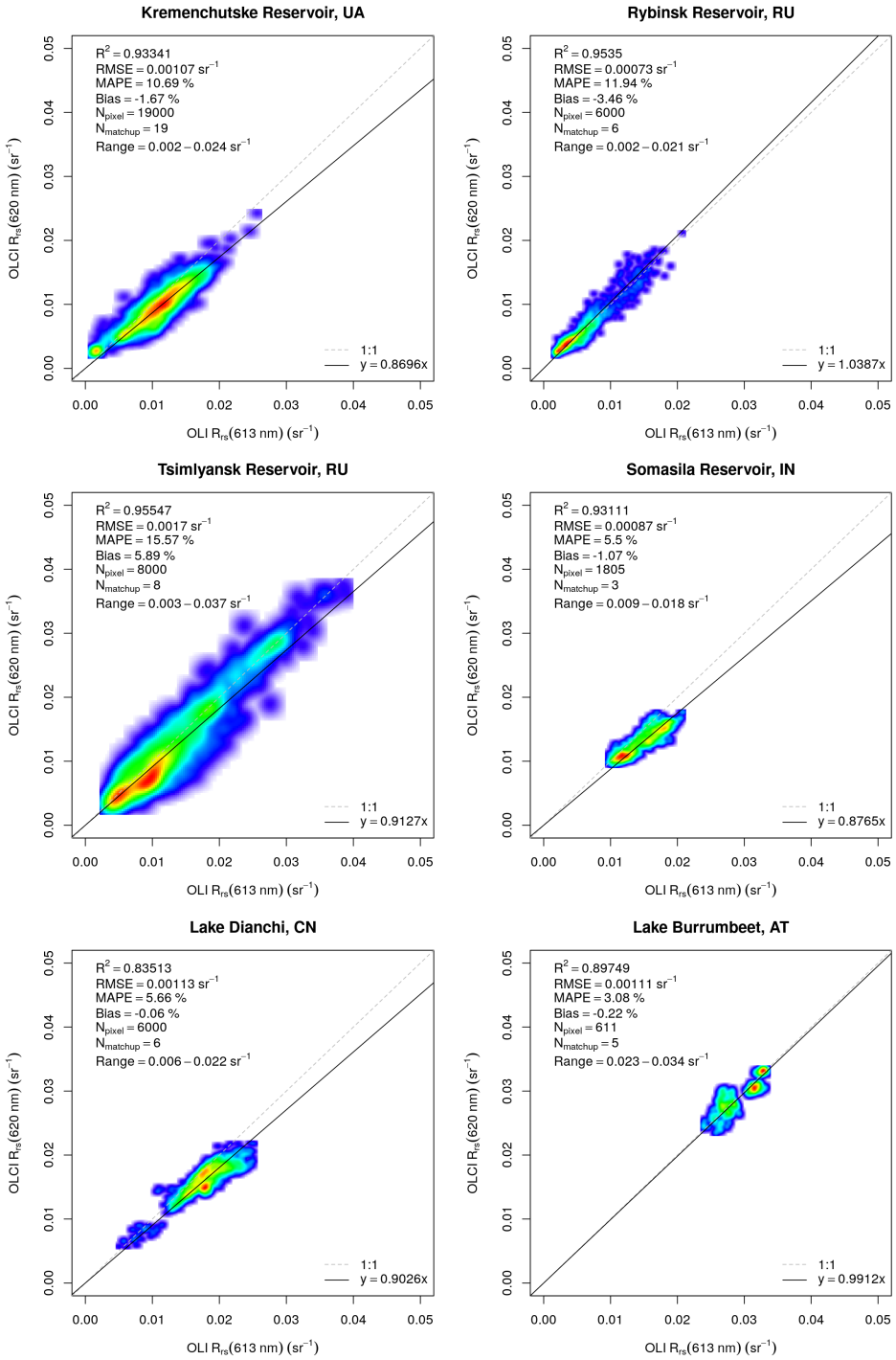

Figure S5. Performance of R_{rs}^{orange} retrieval of the orange *contra*-band against the OLCI orange band per lake.

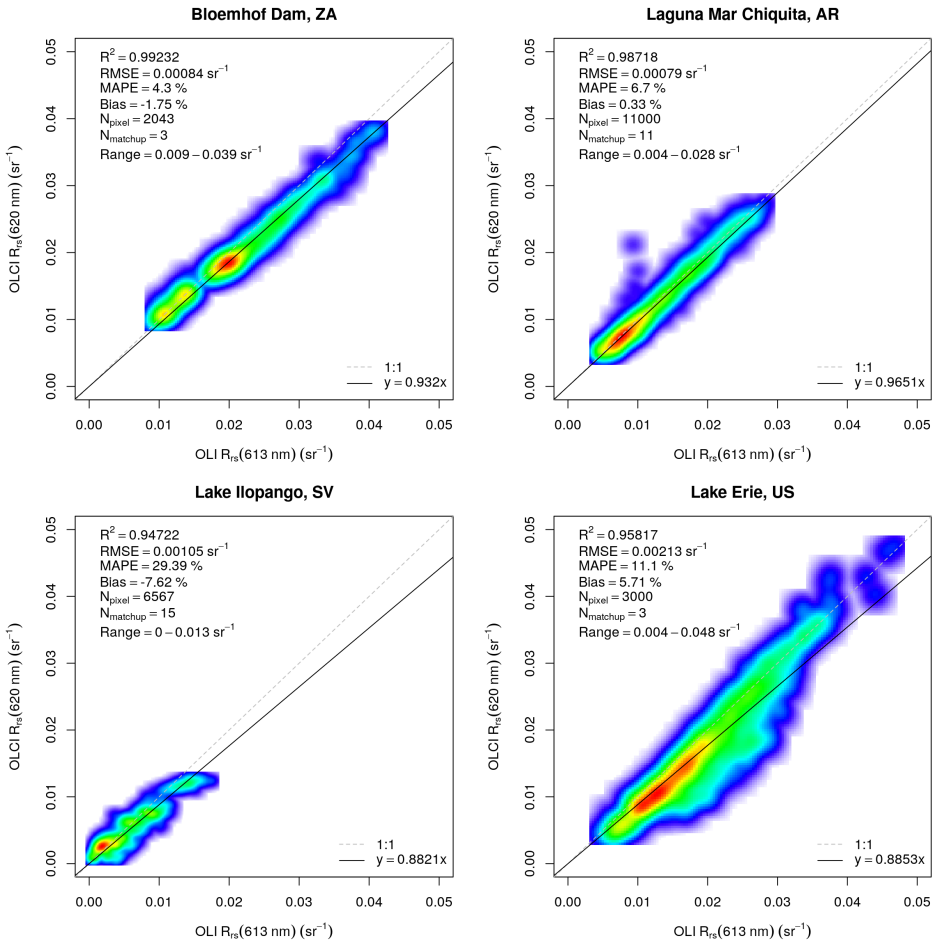

Figure S5. Continued.

Table S1. Details on OLI and OLCI scenes matchup. OLI acquisition time is provided in Coordinated Universal Time (UTC) and time difference to OLCI acquisition is provided in minutes. Also provided are the Sun zenith angle (θ_s) and the aerosol optical thickness at 550 nm ($\tau_a(550)$) estimated with ACOLITE for OLI. Only matchups that passed quality control are numbered in the first column.

Matchup	Lake	Date	UTC Time	Time Diff.	θ_s	$\tau_a(550)$
1	Kremenchuk Reservoir	2016-07-15	08:37:10	12.5	31.31	0.099
2	Kremenchuk Reservoir	2016-07-31	08:37:14	27.6	34.38	0.045
3	Kremenchuk Reservoir	2016-08-07	08:43:26	15.0	36.05	0.087
	Kremenchuk Reservoir	2016-08-23	08:43:32	30.1	40.50	0.383
	Kremenchuk Reservoir	2016-09-08	08:43:37	45.2	45.67	0.113
4	Kremenchuk Reservoir	2016-09-24	08:43:38	60.1	51.29	0.013
	Kremenchuk Reservoir	2017-05-06	08:42:43	66.6	35.00	0.042
5	Kremenchuk Reservoir	2017-06-07	08:43:03	-4.1	29.44	0.118
6	Kremenchuk Reservoir	2017-06-16	08:36:56	23.5	29.07	0.057
7	Kremenchuk Reservoir	2017-07-02	08:37:00	38.5	29.70	0.130
8	Kremenchuk Reservoir	2017-07-18	08:37:04	53.5	31.76	0.107
9	Kremenchuk Reservoir	2017-07-25	08:43:19	41.1	33.06	0.052
10	Kremenchuk Reservoir	2017-08-10	08:43:25	56.1	36.76	0.102
11	Kremenchuk Reservoir	2017-09-04	08:37:20	-2.3	44.25	0.177
12	Kremenchuk Reservoir	2018-05-02	08:36:23	19.2	36.22	0.121
13	Kremenchuk Reservoir	2018-05-25	08:42:17	21.3	31.02	0.093
	Kremenchuk Reservoir	2018-06-10	08:42:14	36.2	29.34	0.109
14	Kremenchuk Reservoir	2018-06-26	08:42:25	51.4	29.34	0.108
	Kremenchuk Reservoir	2018-07-12	08:42:33	66.5	30.87	0.049
15	Kremenchuk Reservoir	2018-08-06	08:36:34	8.1	35.74	0.067
16	Kremenchuk Reservoir	2018-08-13	08:42:49	-4.3	37.54	0.026
17	Kremenchuk Reservoir	2018-08-22	08:36:42	23.2	40.10	0.056
18	Kremenchuk Reservoir	2018-08-29	08:42:56	10.7	42.26	0.264
19	Kremenchuk Reservoir	2018-09-14	08:43:01	25.7	47.60	0.068
20	Rybinsk Reservoir	2016-05-05	08:27:52	66.1	43.29	0.105
21	Rybinsk Reservoir	2016-08-09	08:28:17	55.3	44.35	0.051
22	Rybinsk Reservoir	2017-06-09	08:27:55	36.1	36.95	0.001
23	Rybinsk Reservoir	2017-07-11	08:28:03	66.2	38.12	0.008
24	Rybinsk Reservoir	2017-08-12	08:28:17	-4.6	45.14	0.005
25	Rybinsk Reservoir	2018-07-30	08:27:32	20.8	41.68	0.028
	Rybinsk Reservoir	2018-10-18	08:28:06	-4.9	68.78	0.016
26	Tsimlyansk Reservoir	2016-10-25	08:00:29	20.7	62.28	0.026
	Tsimlyansk Reservoir	2017-05-05	07:59:26	-2.8	35.28	0.104
27	Tsimlyansk Reservoir	2017-05-30	07:53:57	40.3	29.20	0.110
	Tsimlyansk Reservoir	2017-06-06	07:59:47	27.5	29.51	0.058
28	Tsimlyansk Reservoir	2017-08-02	07:54:20	-0.5	33.78	0.064
29	Tsimlyansk Reservoir	2017-08-18	07:54:25	14.6	37.88	0.109
	Tsimlyansk Reservoir	2017-09-10	08:00:15	16.7	46.26	0.242
30	Tsimlyansk Reservoir	2017-09-19	07:54:30	44.6	48.21	0.083
	Tsimlyansk Reservoir	2018-04-06	07:59:32	8.5	45.11	0.053
31	Tsimlyansk Reservoir	2018-04-15	07:53:40	36.3	40.66	0.032
32	Tsimlyansk Reservoir	2018-05-01	07:53:31	51.1	35.43	0.023
	Tsimlyansk Reservoir	2018-06-18	07:53:17	-5.2	28.18	0.051
	Tsimlyansk Reservoir	2018-08-05	07:53:42	40.1	34.47	0.074

Table S1 – Continued.

Matchup	Lake	Date	OLI Time	Time Diff.	θ_s	$\tau_a(550)$
	Tsimlyansk Reservoir	2018-08-12	07:59:33	27.2	37.27	0.069
	Tsimlyansk Reservoir	2018-08-21	07:53:50	55.1	38.72	0.071
33	Tsimlyansk Reservoir	2018-08-28	07:59:40	42.3	41.93	0.103
	Tsimlyansk Reservoir	2018-09-13	07:59:45	57.3	47.25	0.090
	Somasila Reservoir	2016-08-20	05:04:23	26.4	24.96	0.390
34	Somasila Reservoir	2016-11-24	05:04:38	15.4	40.89	0.206
	Somasila Reservoir	2016-12-26	05:04:31	45.2	44.96	0.245
	Somasila Reservoir	2017-03-16	05:04:00	18.5	31.23	0.298
	Somasila Reservoir	2017-04-01	05:03:52	33.3	27.30	0.525
	Somasila Reservoir	2018-03-03	05:03:58	44.6	34.87	0.119
	Somasila Reservoir	2018-05-06	05:03:24	2.9	23.37	0.371
35	Somasila Reservoir	2019-01-01	05:04:09	26.0	45.09	0.153
	Somasila Reservoir	2019-01-17	05:04:07	40.9	44.28	0.309
36	Somasila Reservoir	2019-02-18	05:04:01	9.2	38.39	0.231
37	Lake Dianchi	2016-10-05	03:35:15	33.7	35.36	0.159
38	Lake Dianchi	2017-01-09	03:35:10	22.4	52.52	0.018
39	Lake Dianchi	2017-05-01	03:34:15	25.2	23.19	0.140
40	Lake Dianchi	2018-03-01	03:34:41	6.9	41.15	0.061
	Lake Dianchi	2018-04-02	03:34:25	36.6	30.46	0.270
41	Lake Dianchi	2019-01-31	03:34:45	18.1	49.34	0.117
42	Lake Dianchi	2019-02-16	03:34:43	33.0	45.27	0.079
	Lake Burrumbeet	2016-11-17	00:16:09	-59.8	31.55	0.071
	Lake Burrumbeet	2017-01-29	00:09:42	-45.8	37.37	0.029
43	Lake Burrumbeet	2017-02-21	00:15:43	-48.1	42.46	0.045
	Lake Burrumbeet	2017-03-09	00:15:36	-62.9	46.47	0.145
	Lake Burrumbeet	2017-09-17	00:15:56	-40.8	49.47	0.144
	Lake Burrumbeet	2017-10-03	00:16:03	-55.9	43.57	0.072
	Lake Burrumbeet	2017-11-29	00:09:47	-27.2	30.58	0.126
	Lake Burrumbeet	2017-12-15	00:09:48	-42.1	30.78	0.053
	Lake Burrumbeet	2017-12-31	00:09:47	-57.1	32.37	0.105
44	Lake Burrumbeet	2018-01-23	00:15:47	-59.3	36.16	0.099
45	Lake Burrumbeet	2018-11-16	00:09:34	-52.9	31.82	0.047
46	Lake Burrumbeet	2019-01-19	00:09:27	-52.8	35.40	0.156
47	Lake Burrumbeet	2019-02-27	00:15:30	-30.9	43.83	0.178
	Bloemhof Dam	2017-01-15	08:09:03	34.4	31.09	0.086
	Bloemhof Dam	2017-01-31	08:08:57	49.3	33.35	0.049
48	Bloemhof Dam	2017-04-05	08:08:27	7.6	45.64	0.155
	Bloemhof Dam	2017-04-21	08:08:17	22.4	49.54	0.039
	Bloemhof Dam	2017-08-18	08:15:08	14.3	51.03	0.119
49	Bloemhof Dam	2017-08-27	08:09:00	41.9	48.27	0.037
	Bloemhof Dam	2017-09-03	08:15:11	29.3	45.97	0.064
	Bloemhof Dam	2017-09-19	08:15:14	44.3	40.46	0.040
	Bloemhof Dam	2017-10-30	08:09:12	0.9	28.59	0.046
50	Bloemhof Dam	2017-12-01	08:09:03	30.7	26.33	0.173
	Bloemhof Dam	2017-12-24	08:15:16	33.2	28.24	0.056
	Bloemhof Dam	2018-01-09	08:15:11	48.0	30.26	0.036
	Bloemhof Dam	2018-04-15	08:14:23	36.0	48.03	0.079

Table S1 – Continued.

Matchup	Lake	Date	OLI Time	Time Diff.	θ_s	$\tau_a(550)$
	Bloemhof Dam	2018-09-15	08:08:31	-3.6	42.02	0.057
	Bloemhof Dam	2018-10-24	08:14:58	13.9	29.96	0.043
	Bloemhof Dam	2018-11-02	08:08:49	41.5	28.18	0.016
	Bloemhof Dam	2018-11-09	08:15:01	29.0	27.19	0.071
	Bloemhof Dam	2018-11-25	08:15:00	43.9	26.28	0.096
	Bloemhof Dam	2018-12-27	08:14:57	12.4	28.61	0.013
	Bloemhof Dam	2019-01-05	08:08:46	0.4	29.74	0.078
	Bloemhof Dam	2019-01-12	08:14:56	27.3	30.67	0.066
51	Laguna Mar Chiquita	2016-08-07	14:02:00	9.7	56.38	0.007
52	Laguna Mar Chiquita	2016-08-23	14:02:06	24.7	51.81	0.020
53	Laguna Mar Chiquita	2016-09-08	14:02:11	39.8	46.43	0.015
54	Laguna Mar Chiquita	2017-03-19	14:01:38	16.7	43.83	0.022
55	Laguna Mar Chiquita	2017-04-20	14:01:22	46.4	51.83	0.004
56	Laguna Mar Chiquita	2017-11-14	14:02:13	39.7	27.87	0.176
57	Laguna Mar Chiquita	2017-11-30	14:02:07	54.6	27.22	0.067
58	Laguna Mar Chiquita	2018-02-02	14:01:50	13.2	34.78	0.054
59	Laguna Mar Chiquita	2018-03-06	14:01:37	42.9	40.86	0.088
60	Laguna Mar Chiquita	2018-10-16	14:01:49	50.4	33.82	0.025
61	Laguna Mar Chiquita	2019-02-05	14:01:44	54.1	35.27	0.104
	Lake Ilopango	2016-07-14	16:17:53	34.1	25.93	0.181
62	Lake Ilopango	2016-10-02	16:18:11	8.2	28.51	0.076
63	Lake Ilopango	2017-02-07	16:17:55	26.6	40.71	0.055
	Lake Ilopango	2017-02-23	16:17:50	41.5	36.82	0.495
	Lake Ilopango	2017-08-18	16:18:00	4.3	25.01	0.170
64	Lake Ilopango	2017-12-08	16:18:05	8.1	43.39	0.113
65	Lake Ilopango	2017-12-24	16:18:07	23.1	44.90	0.037
66	Lake Ilopango	2018-01-09	16:18:02	37.9	44.83	0.054
67	Lake Ilopango	2018-03-30	16:17:24	11.1	27.71	0.181
68	Lake Ilopango	2018-07-20	16:17:08	14.6	26.02	0.162
69	Lake Ilopango	2018-08-05	16:17:17	29.7	25.54	0.069
70	Lake Ilopango	2018-10-24	16:17:49	3.9	33.49	0.045
71	Lake Ilopango	2018-11-09	16:17:52	18.9	37.52	0.049
72	Lake Ilopango	2018-12-11	16:17:49	48.9	43.78	0.040
73	Lake Ilopango	2018-12-27	16:17:49	2.3	45.03	0.042
74	Lake Ilopango	2019-01-12	16:17:47	17.3	44.68	0.101
75	Lake Ilopango	2019-02-13	16:17:41	47.1	39.49	0.126
76	Lake Ilopango	2019-03-17	16:17:31	37.3	30.99	0.136
77	Lake Erie	2017-09-26	16:16:45	23.2	46.00	0.021
78	Lake Erie	2018-05-08	16:15:38	29.6	29.42	0.039
79	Lake Erie	2018-05-24	16:15:26	41.3	26.38	0.154
	Lake Erie	2018-09-29	16:16:16	60.8	46.98	0.005

1. Balch, W.M.; Drapeau, D.T.; Bowler, B.C.; Lyczskowski, E.; Booth, E.S.; Alley, D. The contribution of coccolithophores to the optical and inorganic carbon budgets during the Southern Ocean Gas Exchange Experiment: New evidence in support of the "Great Calcite Belt" hypothesis. *Journal of Geophysical Research* **2011**, *116*, C00F06. doi:10.1029/2011JC006941.

2. Dierssen, H.M.; Zimmerman, R.C.; Drake, L.A.; Burdige, D. Benthic ecology from space: optics and net primary production in seagrass and benthic algae across the Great Bahama Bank. *Marine Ecology Progress Series* **2010**, *411*, 1–15. doi:10.3354/meps08665.
3. Gould, R.W.; Arnone, R.A.; Sydor, M. Absorption, Scattering, and Remote-Sensing Reflectance Relationships in Coastal Waters: Testing a New Inversion Algorithm. *Journal of Coastal Research* **2001**, *17*, 328–341.
4. Dierssen, H.M.; Bostrom, K.J.; Chlus, A.; Hammerstrom, K.; Thompson, D.; Lee, Z. Pushing the Limits of Seagrass Remote Sensing in the Turbid Waters of Elkhorn Slough, California. *Remote Sensing* **2019**, *11*, 1664. doi:10.3390/rs11141664.
5. Moore, T.S.; Mouw, C.B.; Sullivan, J.M.; Twardowski, M.S.; Burtner, A.M.; Ciochetto, A.B.; McFarland, M.N.; Nayak, A.R.; Paladino, D.; Stockley, N.D.; Johengen, T.H.; Yu, A.W.; Ruberg, S.; Weidemann, A. Bio-optical Properties of Cyanobacteria Blooms in Western Lake Erie. *Frontiers in Marine Science* **2017**, *4*, 1–20. doi:10.3389/fmars.2017.00300.